International Journal of Biological Macromolecules 185 (2021) 750–760

Contents lists available at ScienceDirect

International Journal of Biological Macromolecules

journal homepage: www.elsevier.com/locate/ijbiomac

In silico, theoretical biointerface analysis and *in vitro* kinetic analysis of amine compounds interaction with acetylcholinesterase and butyrylcholinesterase

Saravanan Kandasamy [a,b], Chitra Loganathan [c], Penislusshiyan Sakayanathan [c], Subramani Karthikeyan [d], Arputharaj David Stephen [e], Dinesh Kumar Marimuthu [c], Saravanan Ravichandran [c], Vignesh Sivalingam [c], Palvannan Thayumanavan [c,*]

[a] *Faculty of Chemistry, University of Warsaw, Ludwika Pasteura 1, Warsaw 02093, Poland*
[b] *Molecular Biophysics Unit, Indian Institute of Science, Bangalore 560 012, India*
[c] *Department of Biochemistry, Periyar University, Salem, Tamil Nadu 636011, India*
[d] *G. S. Gill Research Institute, Guru Nanak College (Autonomous), Chennai 600 042, India*
[e] *Department of Physics, PSG College of Arts and Science, Coimbatore, Tamil Nadu 636014, India*

ARTICLE INFO

Keywords:
Acetylcholinesterase
Butyrylcholinesterase
Hirshfeld surface analysis
Molecular dynamics simulation
Electron density calculation

ABSTRACT

Acetylcholinesterase (AChE) and butyrylcholinesterase (BChE) are considered important target for drug design against Alzheimer's disease. In the present study *in silico* analysis; theoretical analysis of biointerface between ligand and interacting amino acid residues of proteins; and *in vitro* analysis of enzyme inhibition kinetics were carried out to delineate the inhibitory property of amine compounds against AChE/BChE. High throughput virtual screening of amine compounds identified three compounds (2-aminoquinoline, 2-aminobenzimidazole and 2-amino-1-methylbenzimidazole) that best interacted with AChE/BChE. Molecular docking analysis revealed the interaction of these compounds in the active site gorge of AChE/BChE, in particular with amino acid residues present in the peripheral anionic site. Molecular dynamics simulation confirmed the stable binding of these compounds with AChE/BChE. Binding energy calculated through MMGBSA method identified the non-covalent interactions (electrostatic and Van der Waals interactions) have contributed to the stable binding of the amine compounds with the AChE/BChE. Biointerface between amine compounds and AChE/BChE were visualized through Hirshfeld surface analysis. The inter-fragment interaction energies for the possible contacts between amine compounds and amino acid residues were carried out for the first time. All the amine compounds showed mixed-type of inhibition with moderate Ki value in *in vitro* analysis.

1. Introduction

Alzheimer's disease (AD) is the foremost cause of dementia in elderly population and may contribute to 60-70% of cases. Dysfunction of cholinergic neurotransmission in the brain contributes to the salient cognitive decline in AD. Acetylcholinesterase (AChE) is the predominant enzyme present in the brain and hydrolyzes the neurotransmitter acetylcholine (ACh). Nevertheless, butyrylcholinesterase (BChE) is considered pseudo cholinesterase which hydrolyzes different type of choline esters. BChE is mainly present in glial cell and endothelial cells in the brain. In AD brain, the level of ACh is decreased, hence inhibition of AChE is considered important therapeutic target to overcome AD. In addition, the role of BChE in the progression of AD has been identified and inhibition of BChE is gaining importance. Both AChE and BChE are detected among neurofibrillary tangles and neuritic plaques present in the AD brain [1,2]. Amyloid beta (Aβ) aggregation is important hallmark of AD brain. It is found that both AChE and BChE are involved in aggregation of Aβ peptide in AD brain [3–5]. The toxicity induced by AChE complexed with Aβ aggregates is high and in turn it depends on amount of AChE bound to the complex [6,7]. The binding of BChE with Aβ differentiate AD pathology from plaques present in the brains of individuals without dementia [8]. In addition, the major globular tetrameric form of AChE (G4) which is predominant in healthy brain is decreased during the onset of AD, while the minor species (G1;

* Corresponding author at: Department of Biochemistry, Periyar University, Salem, Tamil Nadu 636011, India.
E-mail address: pal2912@periyaruniversity.ac.in (P. Thayumanavan).

https://doi.org/10.1016/j.ijbiomac.2021.06.176
Received 13 April 2021; Received in revised form 10 June 2021; Accepted 25 June 2021
Available online 1 July 2021
0141-8130/© 2021 Published by Elsevier B.V.

monomers and G2; dimers) is unaltered and lead to apparent increase in the lower species to G4 AChE ratio in the AD brain [9–12]. Also, in the plasma of AD patients, the level of G1 and G2 forms were found to be increased [13]. All these studies point to the fact that a molecule which could inhibit BChE and all the molecular forms of AChE could be an ideal candidate to further study for its effect against AD.

For the design of new AChE and BChE inhibitors, the structural knowledge of AChE and BChE is essential. The active site of AChE is placed near the bottom of a 20 Å narrow gorge and 14 aromatic residues lining a substantial portion of the surface [14]. The active site of AChE contains different subsites such as: (1) the catalytic triad Ser203, His447, and Glu334 which is located at the bottom of the gorge; (2) an oxyanion hole Gly121, Gly122 and Ala204 that stabilizes the tetrahedral intermediate binding of the carbonyl group; (3) an acyl binding pocket Phe295, Phe297, Trp236 and Phe338 that binds with the acetyl group of ACh or alkyl moiety of carbamate derivates; (4) an anionic binding site Trp86, Glu202, Tyr133, Gly448 and Ile451 that contains a small number of negative charges but many aromatic residues; (5) a peripheral anionic site (PAS) Asp74, Tyr124, Ser125, Trp286, Tyr337 and Tyr341 was found at the gorge mouth of active site entrance [15]. BChE displays the similar structure to that of AChE and serine amino acid is essential for its catalytic activity [14,16]. However, the two enzymes differ by the presence and extent of subdomains within the gorge. The principal contributors are the peripheral anionic site (Asp70), the choline binding pocket (Trp82), acyl binding pocket (Trp231, Leu286 and Val288) and the catalytic site (Ser198, Glu325 and His438).

In the present study, high throughput virtual screening (HTVS) of about 322 amine compounds present in in-house built library against human AChE and BChE was performed. The top scored three amine compounds namely 2-aminoquinoline (2AQ), 2-aminobenzimidazole (2AB) and 2-amino-1-methylbenzimidazole (2AMB) that interacted with human AChE and human BChE were further analyzed. Molecular docking and molecular dynamics (MD) simulation were performed to understand the intermolecular interaction, binding affinity and molecular flexibility of these compounds in the active site gorge of human AChE and BChE. Molecular mechanics, the generalized Born model and solvent accessibility (MMGBSA) method were employed to elicit the free energies for the binding of these compounds with human AChE and BChE. The density functional theory (DFT) calculation was applied to determine the molecular and atomic level interaction between amine compounds and amino acids present in proteins (AChE and BChE). DFT was also done to understand the energy level required for the binding of the ligand with the protein. To further understand the inhibitory potential of amine compounds, the *in vitro* inhibitory kinetic analysis was carried out against AChE and BChE. Since, various globular forms of AChE is involved in progression of AD, the inhibition of amine compounds against AChE from various sources which is enriched with particular globular form of AChE, electric eel AChE as G4 form [17] and human erythrocyte AChE as G2 form [18] was studied. This is the first study that report the *in silico* (molecular docking and MD), theoretical calculation (DFT) and *in vitro* (inhibition kinetics) analysis of amine compounds interactions with AChE and BChE to understand the bio-interface between inhibitor molecules and amino acids of AChE/BChE.

2. Materials and methods

2.1. Materials

AChE from *Electrophorus electricus*, acetylthiocholine iodide (ATCI), butyrylthiocholine iodide (BTCI), 1,5-bis(4-allyl-dimethylammo-nium-phenyl) pentan-3-one-dibromide (BW284c51), 2AQ, 2AB and 2AMB were purchased from Sigma Chemical Company, USA. 5, 5′-Dithio-bis (2-Nitrobenzoic acid) (DTNB) was purchased from Himedia Pvt. Ltd., India.

2.2. High throughput virtual screening (HTVS)

The crystal structures of AChE (PDB ID: 4EY6) and BChE (PDB ID: 1P0I) proteins were retrieved from Protein Data Bank [19,20]. The crystallographic water molecules within 5 Å to the active site gorge were retained. The hydrogen atoms, charges, and formal bond orders were added by protein preparation wizard (Schrodinger suite). Energy minimization was carried out using the force field OPLS_2005 (Optimized Potentials for Liquid Simulations). About 322 amine fragments present in in-house library were energy minimized by OPLS_2005 force field from LigPrep incorporated in Schrodinger suite-2018 [21]. Grid was generated around the active site residues of AChE and BChE. In the virtual screening process, three different mode of molecular docking was performed that is, all the selected compounds were docked by HTVS mode, then, top scored compounds were subjected automatically to standard precision (SP) docking and then again top scored compounds were taken to extra precision (XP) docking.

2.3. Molecular docking analysis

Molecular docking of top three compounds (2AQ, 2AB and 2AMB) with AChE/BChE have been carried out by induced fit docking (IFD) with extra precision (XP) method using the software package of Schrödinger suite 2018. The intermolecular interactions (hydrogen bonding and hydrophobic interactions) and 2D view of the protein-ligand complex was analyzed using PyMol software [22].

2.4. Molecular dynamics and free energy calculation

To understand the stability of the intermolecular interactions and conformational changes, root mean square deviation (RMSD) and root mean square fluctuation (RMSF) of 2AQ-AChE/BChE, 2AB-AChE/BChE and 2AMB-AChE/BChE complexes were monitored by MD simulation using OPLS3e force field implemented in Desmond v5 package [23]. The periodic precondition with 10 $Å^3$ orthorhombic boxes was built. TIP3P water association system was used as the buffer system. To neutralize the Ewald charge summation, charged ions (Na^+/Cl^-) were placed isotopically. The system was minimized using steepest descent and conjugated gradient methods and heated from 0 to 300 K at 200 ps with the maintenance of canonical ensemble (NVT). Finally, the MD production of the complex system was subjected up to 50 ns in 2 fs time step with isothermal-isobaric ensemble (NPT), constant temperature (300*K*) and pressure (1 bar). The fractions 5, 10, 15, 20, 25, 30, 35, 40, 45 and 50 ns were used to determine the binding free energy (MMGBSA) of the protein-ligand complexes by Prime application available in Schrodinger software package.

2.5. Quantum crystallography studies

Hirshfeld surface analysis was performed to visualize the short contacts between AChE/BChE and amine compounds using *CrystalExplorer 17.5* [24] and then the interfragment interaction energies for the possible contacts were carried out. Single point energy calculation was carried out with DFT/B3LYP method and 6-311G** level of basis set using GAUSSIAN09 software [25] to understand the topological and the electrostatic properties of ligand and the interacting residues around 4 Å of each complex. The topological properties of electron density at the bond critical point (bcp) of the molecules from Bader's quantum theory of atoms in molecules (AIM) were calculated. The Laplacian of electron density $\nabla^2\rho_{cp}(r)$ of the non-covalent bonds were mapped using wfn2plot and denprop available in XD2016 software [26]. Non-Covalent interaction was analyzed to collect reduced gradient scatter (RDG) points by Multiwfn software [27] and drawn by gnuplot program. To calculate the RDG of electron density, the 3D electron density grids were generated for the strong interactions between selected protein and ligands using VMoPro, which were fed into the NCImilano program [28]. These

Table 1
Details of docking score and intermolecular interactions obtained for amine compounds/AChE and amine compounds/BChE enzymes complexes from IFD. Interaction energies were calculated from the counterpoise method.

Protein	Ligand	Intermolecular interactions (D–H···A)	Distance (Å)	Docking score	Glide energy (kcal/mol)	Interaction energy (kcal/mol)
AChE	2-AQ	N•••H-N (Phe295)	2.1	−8.588	−29.132	−1.51
		N-H···O (Ser293)	2.3			−0.92
		N-H···O (Arg296)	2.0			−2.82
	2-AB	N•••H-N (Phe295)	2.0	−9.188	−30.828	−3.02
		N-H···O (Ser293)	2.1			−3.83
		N-H···O (Arg296)	1.9			−2.75
	2-AMB	N•••H-N (Phe295)	2.1	−8.718	−31.331	−3.48
		N-H···O (Ser293)	2.2			−1.38
		N-H···O (Arg296)	1.8			−1.19
BChE	2-AQ	N–H•••O (Ser287)	1.7	−7.641	−25.478	3.84
	2-AB	N•••H-O (Glu197)	1.7	−7.367	−30.660	−8.50
		N-H···O (Tyr128)	2.2			−2.54
		N-H···O (Gly115)	2.0			−1.13
	2-AMB	N•••H-O (Glu197)	1.8	−7.868	−29.346	−11.00
		N-H···O (Glu197)	2.7			

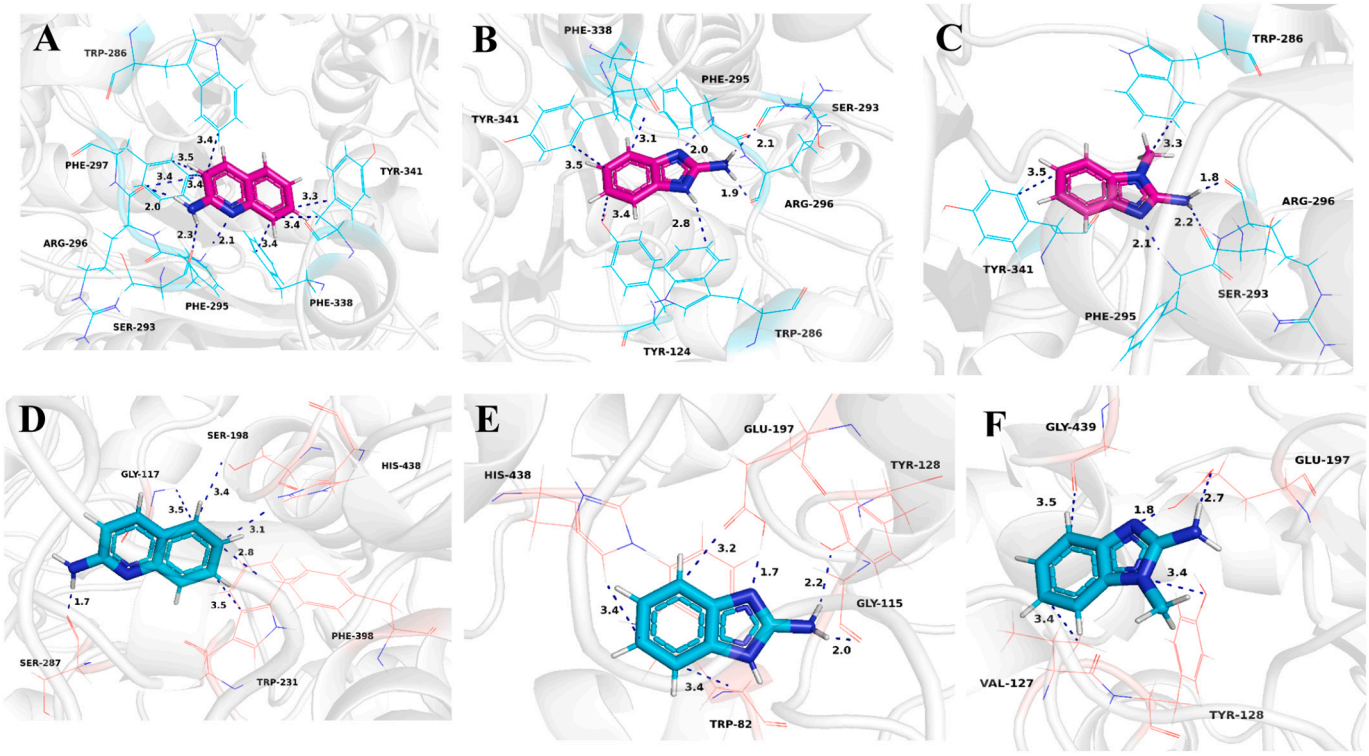

Fig. 1. Intermolecular interactions of amine compounds in the active site of AChE [2AQ/AChE (A); 2AB/AChE (B); 2AMB/AChE (C)] and BChE [2AQ/BChE (D); 2AB/BChE (E); 2AMB/BChE (F)].

electron densities were used to visualize the non-covalent interactions (NCI) isosurface by MolIso software [29].

2.6. Enzymes preparation

AChE from *E. electricus* was used without further purification. Detergent soluble AChE from human erythrocyte was prepared by homogenizing erythrocyte ghost using potassium phosphate (KPO_4) buffer (50 mM), pH 7.4 containing 0.2%, triton X-100 [30]. Human plasma sample was used as source of BChE.

2.7. AChE and BChE enzyme activity and inhibition analysis

AChE and BChE esterase activity was carried out in reaction mixture consisting of 100 mM KPO_4 buffer (pH 7.0; containing 100 μM BW284c51, specific inhibitor of AChE for BChE assay), 2 mM DTNB, 1 mM ATCI (for AChE assay) or 3 mM BTCI (for BChE assay) and an aliquot of enzyme in a total volume of 1000 μl with distilled water. After incubating the reaction mixture at 37 °C for 10 min (for AChE assay) or 5 min (for BChE assay), the reaction was terminated by addition of 500 μl of 0.5 mM eserine hemisulphate [31]. The yellow color formed was measured at 412 nm using UV visible spectroscopy (UV-1800, Shimadzu, Koyota, Japan).

The stock solution of 2AQ, 2AB and 2AMB (100 mM) was prepared in dimethylsulphoxide (DMSO). About 10 mM solution of 2AQ, 2AB and 2AMB was prepared from stock using distilled water and further used for inhibition assay. For enzyme inhibition assay, the enzyme solution in buffer was incubated with different concentrations of either 2AQ, 2AB or 2AMB at room temperature for 30 min. After incubation, the AChE or BChE enzyme activity was determined as given above.

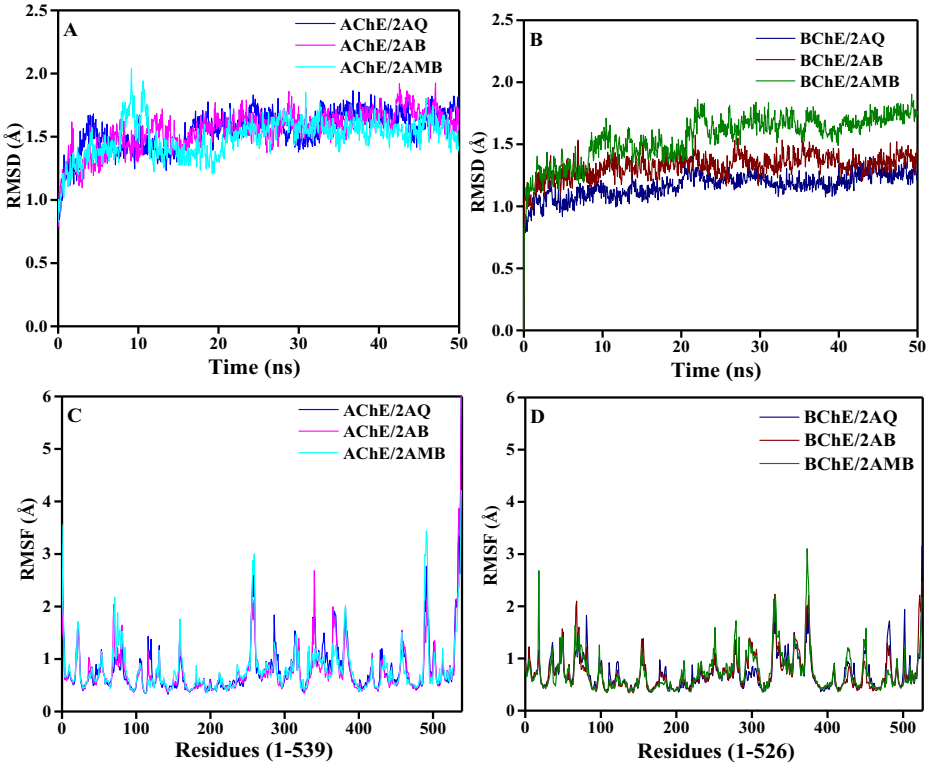

Fig. 2. RMSD (A and B) and RMSF (C and D) of three amine compounds/AChE or BChE complexes throughout MD simulation.

2.8. Kinetic analysis

The kinetics of AChE or BChE inhibition by 2AQ, 2AB or 2AMB was determined using Lineweaver and Burk (LB) double reciprocal plot and Dixon plot [32,33]. AChE enzyme inhibition was determined over a range of ATCI concentrations (0.25 mM to 1.00 mM) in the absence and in the presence of 2AQ, 2AB or 2AMB. For BChE activity, the inhibition was analyzed in the presence of various concentrations (1.5 mM to 3 mM) of BTCI in the absence and in the presence of 2AQ, 2AB or 2AMB. The inhibitory constant (Ki) was determined from the Dixon graph.

All the enzyme activities were carried out in two sets of triplicates and data were presented as mean ± SD.

3. Results and discussion

3.1. Amine compounds complexed with AChE/BChE

HTVS of amine fragments with human AChE and BChE was performed and selected top three compounds (2AQ, 2AB and 2AMB) were subjected to IFD. Different scores and energies of the selected amine compounds and AChE/BChE complexes were obtained and shown in Table 1. The best conformation of amine compounds binding with AChE/BChE was chosen based on docking score and glide energy. All the compounds interacted with almost similar binding score with AChE/BChE. Amine compounds oriented in the active site gorge of AChE and interacted with amino acids such as Ser293, Phe295, Arg296, Trp286 and Tyr341 (Fig. 1A-C; 2D interactions were shown in Fig. S1). Hydrogen bonding, hydrophobic interactions and π–π stacking were found between amine compounds and amino acid residues of AChE. In particular, all three amine compounds interacted with amino acid present in acyl binding site (Phe295) and PAS (Tyr341) regions. Notably in AChE/amine compounds complexes, amine group of 2AQ, 2AB and 2AMB formed strong hydrogen bond interactions with Phe295 (~2.1 Å) and Ser293 (~2.2 Å). Interestingly, both hydrogen atoms of NH_2 group of all amine compounds interacted simultaneously with amino acids Ser293 and Arg296. The phenyl group of the amine compounds formed strong hydrophobic interactions with amino acids (Tyr341 and Trp286) present in PAS. Further, π–π stacking interaction was formed between aromatic ring present in 2AQ and 2AMB molecules with amino acid Phe297.

Similar to AChE, amine compounds were placed in the active site gorge of the BChE. Amine group of 2AB and 2 AMB formed strong hydrogen bonding interactions with active site amino acid Glu197 at a distance of 1.7 and 1.8 Å, respectively; which is not observed in the 2AQ/BChE complex (Figs. 1D-F; S1). Moreover, amine compounds hydrophobically interacted with catalytic site residues Ser198 and His 438. On comparing the superimposed view of both AChE/amine compounds and BChE/amine compounds complexes, all three amine compounds were placed in the similar position in AChE; whereas in BChE, 2AB and 2AMB were placed in anionic subsite region and 2AQ placed slightly far away from the anionic subsite region (Fig. S2). From the docking study, it is important to note that amine compounds interacted with PAS of AChE. The interaction of amine compounds with AChE is similar to that of propidium and 1,10-phenanthroline which was earlier found to be PAS specific inhibitors [34,35]. The PAS of AChE rather than catalytic site is involved in Aβ aggregation. PAS specific inhibitor (propidium) and monoclonal antibodies directed towards PAS has inhibited AChE-induced Aβ aggregation [36,37]. Since, PAS forms the entry site of the active site gorge of AChE and BChE, any compound that bind in this region would sterically block the entry of substrate or alter the anionic subsite thereby the catalytic activity [35]. Hence, interaction of amine compounds with AChE might have dual function: (i) inhibition of AChE catalytic activity; and (ii) inhibition of AChE-induced Aβ aggregation.

3.2. Stability and conformational behavior of amine compounds/AChE or BChE complexes

About 50 ns of MD simulation were performed for the amine compounds/AChE and amine compounds/BChE complexes to explore the

Table 2
Binding free energy of amine compounds interaction with AChE or BChE using Prime/MMGBSA approach.

Complex	dG bind	Coulomb	Covalent	H bond	Lipo	VdW
AChE/2AB	−36.501	−27.54	0.051	−2.227	−9.174	−18.503
AChE/2AM	−41.184	−26.362	0.364	−2.265	−9.771	−20.617
AChE/2AQ	−47.259	−23.585	0.979	−1.923	−14.215	−20.304
BChE/2AB	−34.507	−32.304	0.985	−2.083	−6.348	−17.854
BChE/2AM	−40.057	−20.148	0.969	−1.712	−10.548	−22.495
BChE/2AQ	−23.531	−5.312	0.289	−0.760	−11.000	−23.414

Table 3
Topological parameters of intermolecular interactions obtained from amine compounds and AChE/BChE complexes.

Intermolecular interactions	Distance	$\rho_{cp}(r)$ (eÅ^{-3})	$\nabla^2\rho_{cp}(r)$ (eÅ^{-5})	G(r) (a.u.)	V(r) (a.u.)	H(r) (a.u.)	D kcal/mol
AChE-2AQ							
N•••H-N (Phe295)	2.05	0.166	1.857	0.034	−0.049	−0.015	15.36
N–H•••O (Arg296)	1.95	0.164	2.321	0.037	−0.0497	−0.013	15.59
N–H•••O (Ser293)	2.25	0.083	1.064	0.014	−0.017	−0.003	5.349
AChE-2AB							
N•••H-N (Phe295)	2.14	0.106	1.42	0.02	−0.025	−0.005	7.849
N–H•••O (Ser293)	2.13	0.146	1.587	0.028	−0.0398	−0.012	12.49
N–H•••O (Arg296)	1.82	0.227	3.186	0.058	−0.0827	−0.025	25.94
AChE-2AMB							
N•••H-N (Phe295)	2.14	0.136	1.505	0.026	−0.0357	−0.01	11.2
N–H•••O (Arg296)	2.08	0.132	1.869	0.027	−0.0355	−0.008	11.12
N–H•••O (Ser293)	2.22	0.071	0.894	0.011	−0.0134	−0.002	4.202
BChE-2AQ							
N–H•••O (Ser287)	1.74	0.338	2.666	0.088	−0.1485	−0.06	46.6
BChE-2AB							
N–H•••O (Tyr128)	2.18	0.106	1.304	0.019	−0.0246	−0.006	7.726
N•••H-O (Glu197)	1.72	0.262	3.829	0.072	−0.1042	−0.032	32.71
N–H•••O (Gly115)	1.98	0.158	2.051	0.034	−0.0462	−0.012	14.51
BChE-2AM							
N•••H-O (Glu197)	1.78	0.302	2.507	0.075	−0.1241	−0.049	38.94
N–H•••O (Glu197)	2.80	0.046	0.552	0.006	−0.0069	−6E-04	2.165

stability of the molecules in the protein environment. The RMSD values of the three amine compouds with AChE/BChE remained within 2 Å and all three compounds were found to be highly stable during MD simulation (Fig. 2A and B). The RMSF graph displays the Cα atom fluctuation of all six complexes; in common, loop regions are fluctuated highly than α-helix and β-sheets. The RMSF values are high in N and C-terminal loop residues of amine compounds/AChE complexes whereas in amine compounds/BChE complexes it was less (Fig. 2C and D). It can be mainly attributed to the difference in N and C terminal loop amino acid residues between AChE and BChE. However, the RMSF of active site residues are lesser on compared with other parts of residues present in the proteins. The intermolecular interactions obtained from MD simulation shows that some docking interactions became strong, few interactions found to be vanished and new interactions are formed. Notably, the interaction of Phe295 (73%), Ser293 (89%) and Arg296 (92%) of AChE with 2AB is highly stable during the MD simulation (Fig. S3).

The binding energy of the all six complexes was calculated by MMGBSA method; the values obtained for amine compounds/AChE complexes are −47.259 (2AQ), −36.501 (2AB), −41.184 (2AM), and amine compounds/BChE complexes are −23.531 (2AQ), −34.501 (2AB), −40.057 (2AM) kcal/mol (Table 2). Electrostatic interaction and Van der Waals (VdW) interactions have contributed to the stable binding of the amine compounds with the AChE and BChE. The interaction of functional group NH_2 of amine compounds with amino acids such as Ser, Glu and Tyr present in AChE/BChE has correlated well with the contribution of electrostatic interaction in stable binding of ligand and protein. Although VdW interactions are considered week, the large number of these interactions that occurred upon molecular recognition events of amine compounds with AChE/BChE has made significant contribution to the total free energy [38]. Apart from these energies, lipophilic energy has contributed to overall binding energy of the amine compounds with AChE/BChE. The interaction of phenyl ring of amine compounds with amino acids such as Phe, Tyr and Trp throughout MD simulation has contributed to lipophilic energy and favored intact conformational positioning of amine compounds with AChE/BChE. Altogether all the amine compounds showed stable binding with AChE/BChE along with favorable binding energies.

3.3. Biointerface analysis (topological and electrostatic properties) of interaction between amine compounds and amino acids of AChE or BChE

The understanding of biointerface that is the region of contact between enzymes (AChE or BChE) with ligands (amine compounds) is a key prerequisite for rational drug design. Moreover, the design of drug with improved physical and chemical properties are major driving forces in the medicinal chemistry. To achieve this, quantum crystallographic approach helps to estimate the stability of interactions obtained from the ligand molecule with their target amino acid residues. Indeed, recent methodology development reports [39–42] helped us to study as well as compute intermolecular interaction energies of protein-ligand complexes. Theoretical charge densities [electron density $\rho_{cp}(r)$, Laplacian of electron density $\nabla^2\rho_{cp}(r)$, kinetic energy (Gr), potential energy (Vr), total energy (Hr) and hydrogen bond dissociation energy (D)] of amine compounds interaction with active site amino acid residues were carried out with (3,−1) type of critical point that is stabilized by N–H···O type of interactions (Table 3). Notably, $\rho_{cp}(r)$ (0.227 eÅ^{-3}) and $\nabla^2\rho_{cp}(r)$ (3.186 eÅ^{-5}) of NH_2···O/Arg296 interaction of AChE/2AB complex is stronger compared with other interactions of different complexes

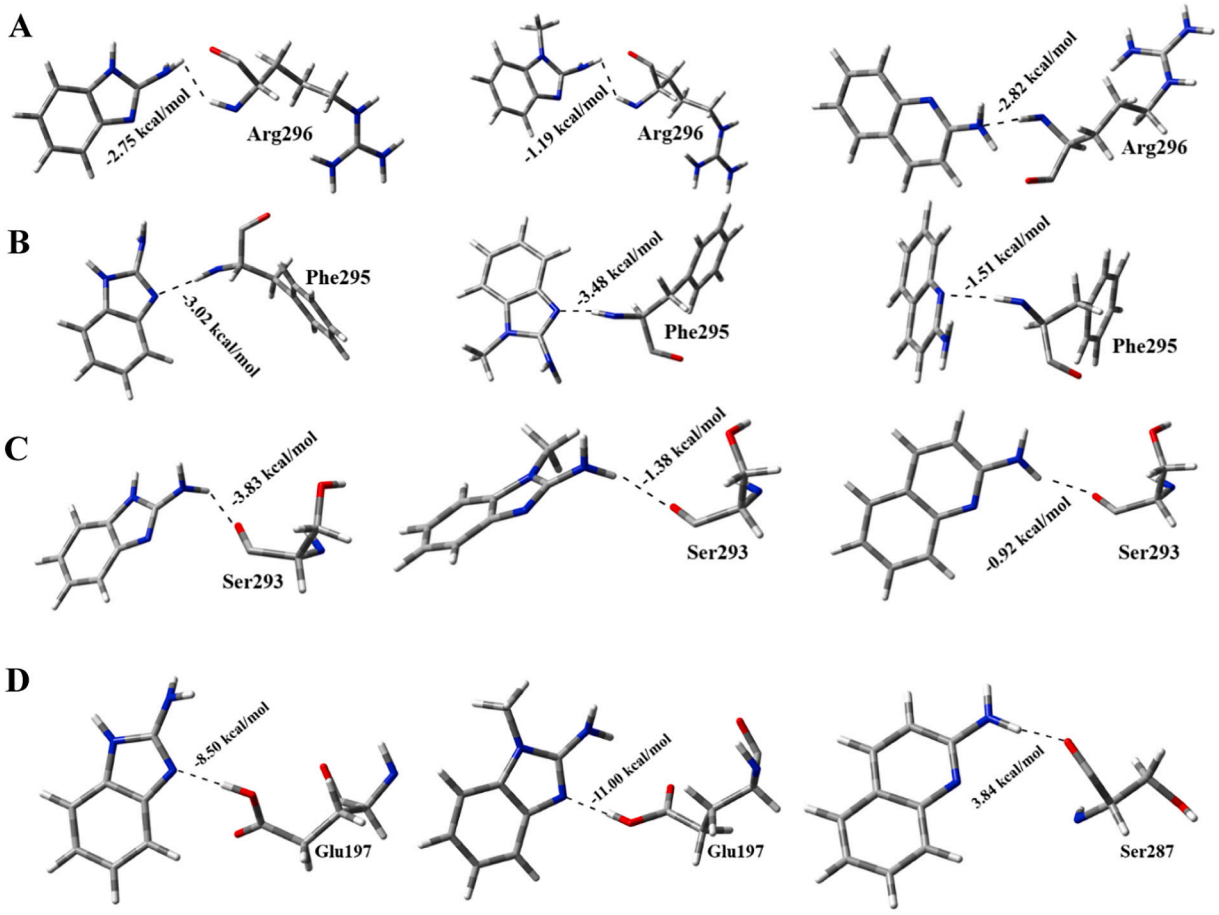

Fig. 3. Interfragment interaction energies (1st) between active site residues of AChE (A to C) and amine compounds as well as active site residues of BChE (D) and amine compounds.

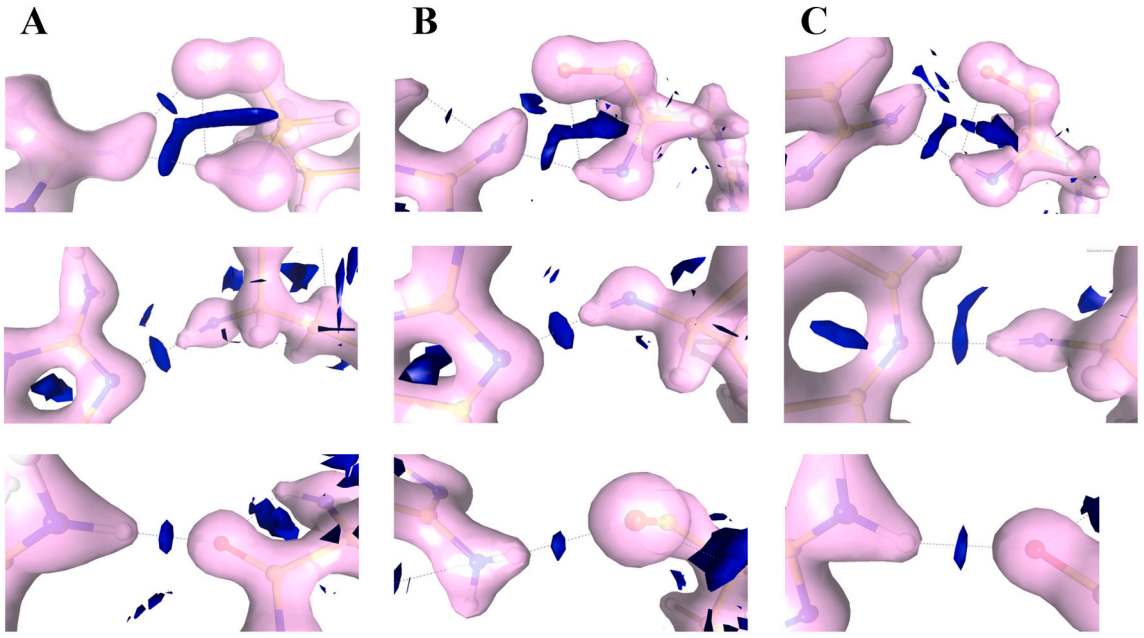

Fig. 4. NCI iso-surfaces of the intermolecular interactions between amino acid of AChE-amine compounds. (A) 2AB, (B) 2AMB, (C) 2AQ with Arg296 (top), Phe295 (middle) and Ser293 (bottom) of AChE.

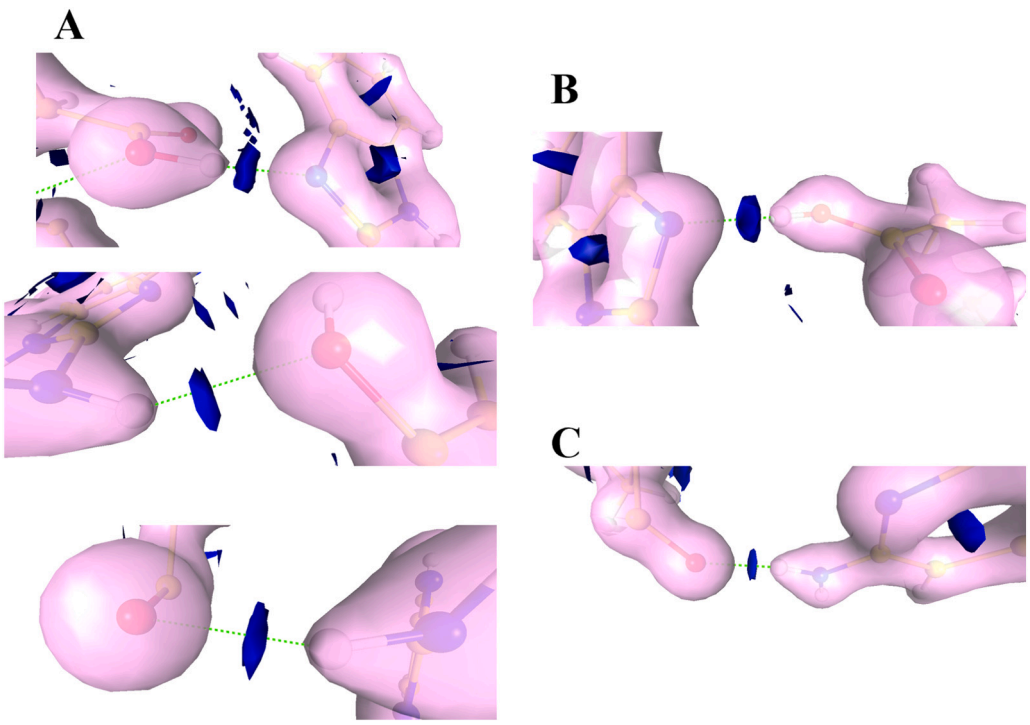

Fig. 5. NCI iso-surfaces of the intermolecular interactions between amino acid of AChE-amine compounds. (A) 2AB with Glu197, Tyr128, Gly115; (B) 2AMB with Glu197, (C) 2AQ with Ser287 of BChE.

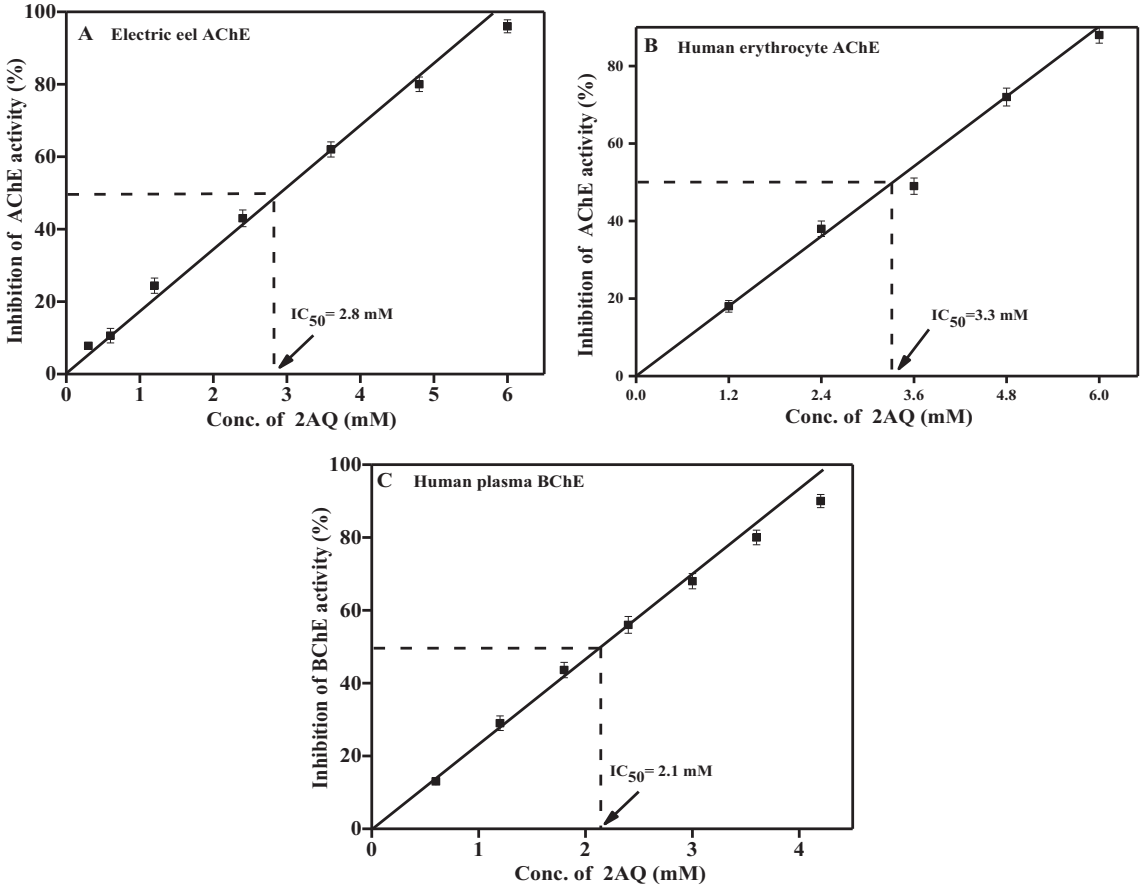

Fig. 6. Inhibition of G4 form (electric eel) AChE (A), G2 form (human erythrocyte) AChE (B) and human plasma BChE (C) by 2AQ. Results are expressed as mean ± SD ($n = 6$).

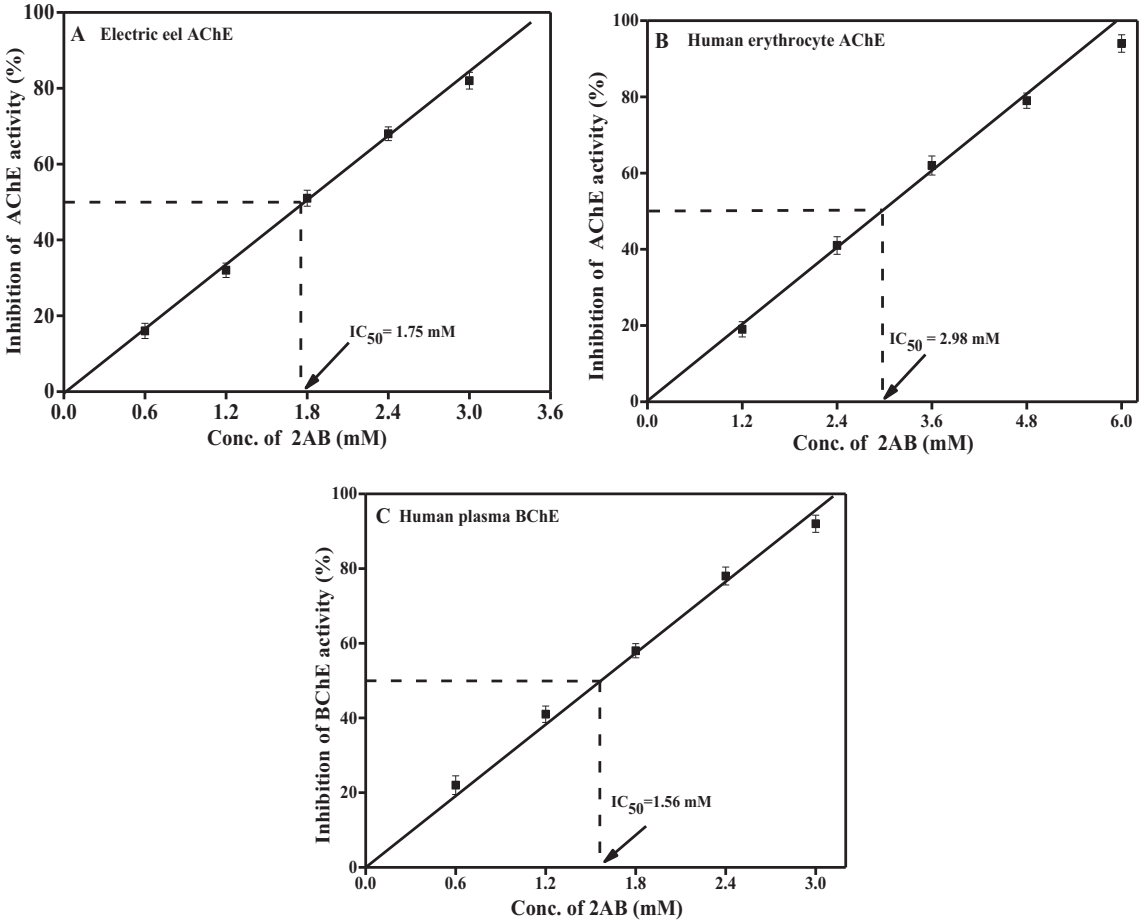

Fig. 7. Inhibition of G4 form (electric eel) AChE (A), G2 form (human erythrocyte) AChE (B) and human plasma BChE (C) by 2AB. Results are expressed as mean ± SD (n = 6).

studied. In the BChE/amine compounds complexes, the $\rho_{cp}(r)$ and $\nabla^2\rho_{cp}(r)$ of $NH_2\cdots O$/Glu197 are 0.267 eÅ^{-3} and 3.829 eÅ^{-5}, respectively. The theoretical electron densities of N–H···O type of interaction are well agreed with the reported results, the values are 0.269 eÅ^{-3} and 3.009 eÅ^{-5} [39], 0.216 eÅ^{-3} and 3.279 eÅ^{-5} [40]. This smaller amount of electron density as well as positive Laplacian of electron densities clearly confirmed that the interactions are the closed-shell interactions and have contributed to the high electron density around the ligand and amino acid residues of the protein. Also, the topological properties of intermolecular interactions were highly correlated with the geometry of interactions. Fig. S4A and B show the deformation and Laplacian of electron density map of intermolecular interactions of AChE amino acid residues Phe295 and Arg296 with 2AB which displayed polarized lone-pairs and charge concentration/depletion at the critical bond of the interactions. Further, electrostatic potential (ESP) maps of intermolecular interactions between different amine compounds and AChE (Fig. S4C) clearly confirmed that amine groups played important role in the formation of new interactions in the protein environment. The iso-surface representation of the molecular ESP map of intermolecular interactions explained the electronegative surface regions and how this occupied between interactions. The ESP of hydrogen bonding interaction revealed the deeper insights of electronic environments in the ligand-protein interactions [39–42]. In line with this, the shared high negative ESP regions were observed at the vicinity of $NH_2\cdots O$/Arg296 and $NH_2\cdots O$/Phe295 region in all three amine compounds interaction site with AChE.

Hirshfeld surface along with subsequent fingerprint maps were plotted to quantify the intermolecular contacts between amine compounds and amino acid residues of AChE/BChE [43]. In the d_{norm} map of all six amine compounds and AChE/BChE complexes, the red surface represents hydrogen bonding interactions, white surface denotes VdW separation and blue surface represents short contact distances (Figs. S5 and S6). Amine group of all three compounds showed strong red surfaces over the amino acids in active site of both AChE and BChE which confirms the hydrogen bonding interactions. In addition, large white surfaces over the amine compounds substantiated the hydrophobic interactions with active site residues. The corresponding fingerprint plot of these complexes displayed sharp spikes ($d_e + d_i \sim 2.2$ Å), which further confirmed the strong hydrogen bond interactions between ligand and protein.

Pair of each residue-ligand was separated to perform NCI energy calculation which is found to be attractive in nature. In the protein-ligand complexes, NCI (hydrogen bonding, hydrophobic, electrostatic and VdW interactions) plays a crucial role. Accurate NCI energies of these bonds are essential to understand the binding mechanism in the formation of drug-receptor complexes [44]. Therefore, NCI descriptor has proved method for the qualitative analysis of hydrogen bonds. The intermolecular interaction energies of amine compounds with selected active site residues (which showed stabilized energy in comparison to other residues) of AChE and BChE are shown in Fig. 3. The interaction energy between amine compounds with different active site residues of AChE ranged from −3.83 to −0.92 kcal/mol (Fig. 3A to C). High stabilized energy were observed between amino acid residue Glu197 of BChE with 2AB (−8.50 kcal/mol) and 2AMB (−11.0 kcal/mol). The total interaction energies of each complexes are −38.21 (AChE/2AQ), −35.82 (AChE/2AB), −33.58 (AChE/2AMB), −38.64 (BChE/2AQ),

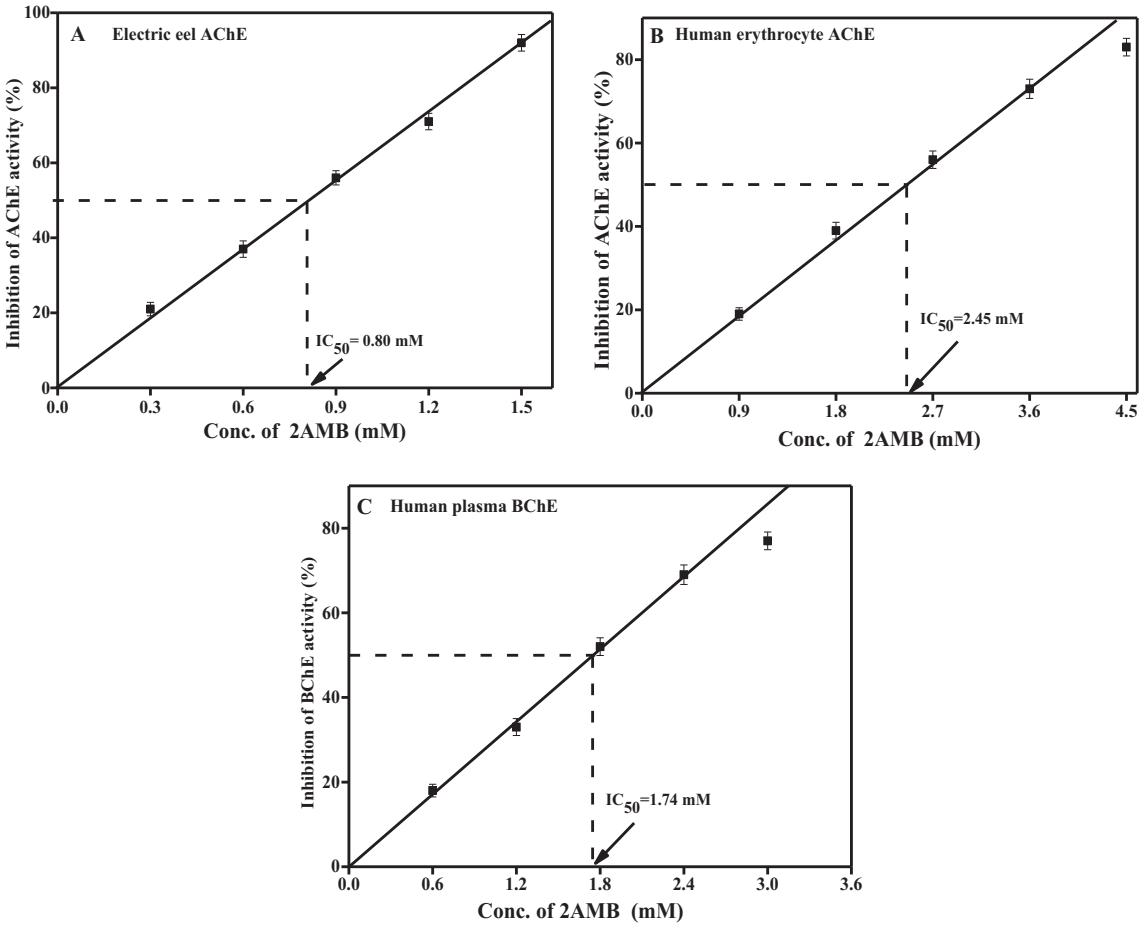

Fig. 8. Inhibition of G4 form (electric eel) AChE (A), G2 form (human erythrocyte) AChE (B) and human plasma BChE (C) by 2AMB. Results are expressed as mean ± SD (n = 6).

Table 4
Summary of IC_{50} and Ki values of all three compounds with AChE and BChE.

Enzyme		2AQ		2AB		2AMB	
		IC_{50} (mM)	Ki	IC_{50}	Ki	IC_{50}	Ki
AChE	Electric eel	2.8	1.15	1.75	1.27	0.80	0.63
	Human erythrocyte	3.3	2.16	2.98	2.78	2.45	1.9
BChE	Human plasma	2.1	1.9	1.56	1.25	1.74	0.92

−40.14 (BChE/2AB) and −30.11 (BChE/2AMB) kcal/mol. This total interaction energies are almost similar to glide energy and binding free energies obtained from the molecular docking and MD simulation. Therefore, the quantum crystallographic based interaction energy calculation is a better alternative to docking score-based modelling.

The electron densities of NCI obtained from the quantum chemical calculation were used to draw the RDG map. Fig. S7 shows the RDG map of all three amine compounds with Arg296 of AChE, Glu197 and Ser287 of BChE. In which, the scatter RDG points are shown in different color, the strong hydrogen bonding interactions are confirmed from the scatter points in blue color, VdW interactions are shown in green scatter points and ring steric effect observed in the red scatter points. On compared with all the interactions, the blue color scatter points are higher in the 2AM of both AChE and BChE complexes than the others which confirm that electron density of these NCI are more stable. Overall, the quantum theory of atoms in molecules and NCI energy calculation for the protein-ligand complexes exhibited an excellent correlation between topological parameters and inter-fragment interaction energies of selected amine compounds in the active site of AChE and BChE. Recently, a study demonstrated the electron density-based analysis of hydrogen bonds involved in the formation of protein secondary structure from quantum crystallographic approaches [45]; however, such analysis for intermolecular NCI between amino acid residues of protein and ligand in protein-ligand complexes has not been attempted. In the present study, for the first time electron density-based analysis of amine compounds interaction with amino acid residues of AChE/BChE was carried out towards drug design perspective. Figs. 4 and 5 show the NCI isosurface map of intermolecular interactions between protein and ligand molecules which clearly visualized the strong and weak interactions. The NCI isosurfaces was found to be well-defined and clearly visible in the vicinity of $NH_2\cdots O$/Arg296 and $NH_2\cdots O$/Phe295 of all three complexes (AChE/amine compounds) which indicates the stronger NCI. However, between amine compounds and amino acid residue Ser293 the isosurface started to diffuse which indicated weaker NCI (Fig. 4). In the amine compounds/BChE complex, the NCI isosurface of Glu 197 of BChE was found to be stronger with 2AB and 2AMB (Fig. 5). Theoretical-based quantum crystallographic approaches used in the present study delineated the topological character and intermolecular interaction energies between protein and ligand biointerface. This approach applied in the present study could be used for rational drug design in the future. Further to substantiate the results obtained from *in silico* and theoretical biointerface analysis, *in vitro* inhibitory potential of amine compounds with AChE and BChE was carried out.

3.4. Inhibition of AChE and BChE in in vitro

All the compounds 2AQ, 2AB and 2AMB showed dose-dependent inhibition against AChE and BChE (Figs. 6, 7 and 8). The IC_{50} values and Ki values of all three compounds with AChE and BChE is summarized in Table 4. The compound 2AQ inhibited electric eel AChE, human erythrocyte AChE and human plasma BChE with IC_{50} value of 2.8 mM, 3.3 mM and 2.1 mM, respectively. The compound 2AQ showed mixed-type (*i.e.* inhibitor binds to free enzyme and enzyme-substrate complex; Vmax decreases and Km increases) of inhibition (Fig. S8A, B and C), with Ki values of 1.15 mM, 2.16 mM and 1.9 mM, respectively as shown in Dixon plot (Fig. S8D, E and F).

The IC_{50} values of 2AB were found to be 1.75 mM, 2.98 mM and 1.56 mM, respectively for electric eel AChE, human erythrocyte AChE and human plasma BChE. The compound 2AB inhibited both AChE and BChE in mixed manner (Fig. S9A, B and C). The Ki values were 1.27 mM, 2.78 mM and 1.25 mM for electric eel AChE, human erythrocyte AChE and human plasma BChE, respectively (Fig. S9D, E and F).

The IC_{50} values of 2AMB against electric eel AChE, human erythrocyte AChE and human plasma BChE were found to be 0.80 mM, 2.45 mM and 1.74 mM, respectively. Kinetic analysis revealed mixed type of inhibition against both AChE and BChE (Fig. S10A, B and C) by 2AMB. The Ki values against electric eel AChE, human erythrocyte AChE and human plasma BChE were found to be 0.63 mM, 1.9 mM and 0.92 mM, respectively (Fig. S10D, E and F).

The amine compounds, 2AQ, 2AB and 2AMB inhibited both the molecular forms of AChE as well as BChE. Kinetic analysis is in line with the results obtained in *in silico* analysis and theoretical analysis, in which amine compounds showed mixed type of inhibition that is, these compounds bound in the active site gorge of both the proteins AChE and BChE. Both AChE and BChE is involved in the progression of AD through ill-effecting the cholinergic neurotransmission and physically affecting Aβ fibril assembly [3–5]. Hence, any molecules that could interact with both AChE and BChE can be used as lead molecule to design AD drug.

4. Conclusion

In the present study, through HTVS, three amine compounds (2AQ, 2AB and 2AMB) were found to bind with AChE and BChE effectively in *in silico*. Further through molecular docking analysis, it was identified that these compounds bound in the active site gorge of both AChE and BChE interacting with amino acid residues present in the PAS. MD analysis showed the stable interaction of amine compounds with the AChE and BChE. Biointerface between amine compounds and AChE/BChE were visualized through Hirshfeld surface analysis which showed the short contacts between AChE/BChE and amine compounds. The inter fragment interaction energies for the possible contacts between amine compounds and AChE/BChE were carried out for the first time. The intermolecular interaction energies were equivalent to the binding energies obtained through MMGBSA analysis. The biointerface analysis carried out in the present study could be used for rational drug design apart from MD simulation. In *in vitro* analysis, all the amine compounds showed mixed type of inhibition with moderate Ki values.

CRediT authorship contribution statement

Author name	Specific role in study
Saravanan Kandasamy	Design, execution, interpretation of study, writing of the manuscript
Chitra Loganathan	Design, execution, interpretation of study, Supervision of the work, writing of the manuscript
Penislusshiyan Sakayanathan	Methodology, execution
Subramani Karthikeyan	*In silico* analysis and interpretation
Arputharaj David Stephen	*In silico* analysis and interpretation
Dinesh Kumar Marimuthu	*In vitro* analysis
Saravanan Ravichandran	*In vitro* analysis
Vignesh Sivalingam	*In vitro* analysis
Palvannan Thayumanavan	Conception and design of the work. Supervision of the work. Correction, review and editing of the manuscript.

(*continued on next column*)

(*continued*)

Declaration of competing interest

All authors declare no conflict of interest.

Acknowledgment

Dr. L. Chitra acknowledges University Grants Commission, India for the award of Dr. D.S. Kothari Postdoctoral Fellowship (Ref. No. F.4-2/2006 (BSR)/BL/17-18/0313). Dr. S. Penislusshiyan acknowledges Human Resource Development, Department of Health Research, Ministry of Health and Family Welfare, India for the award of young scientist fellowship (Ref. No. R.12014/51/2020-HR).

Appendix A. Supplementary data

Supplementary data to this article can be found online at https://doi.org/10.1016/j.ijbiomac.2021.06.176.

References

[1] P. Gómez-Ramos, C. Bouras, M. Moran, Ultrastructural localization of butyrylcholinesterase on neurofibrillary degeneration sites in the brains of aged and Alzheimer's disease patients, Brain Res. 640 (1994) 17–24.
[2] M. Moran, E. Mufson, P. Gomez-Ramos, Colocalization of cholinesterases with ß amyloid protein in aged and Alzheimer's brains, Acta Neuropathol. Commun. 85 (1993) 362–369.
[3] A. Alvarez, F. Bronfman, C.A. Pérez, M. Vicente, J. Garrido, N.C. Inestrosa, Acetylcholinesterase, a senile plaque component, affects the fibrillogenesis of amyloid-ß-peptides, Neurosci. Lett. 201 (1995) 49–52.
[4] N.C. Inestrosa, A. Alvarez, C.A. Perez, R.D. Moreno, M. Vicente, C. Linker, O. I. Casanueva, C. Soto, J. Garrido, Acetylcholinesterase accelerates assembly of amyloid-ß-peptides into Alzheimer's fibrils: Possible role of the peripheral site of the enzyme, Neuron 16 (1996) 881–891.
[5] S. Darvesh, M.K. Cash, G.A. Reid, E. Martin, A. Mitnitski, C. Geula, Butyrylcholinesterase is associated with ß-amyloid plaques in the transgenic APPSWE/PSEN1dE9 mouse model of Alzheimer disease, J. Neuropathol. Exp. Neurol. 71 (2012) 2–14.
[6] A. Alvarez, R. Alarcón, C. Opazo, E.O. Campos, F.J. Muñoz, F.H. Calderón, F. Dajas, M.K. Gentry, B.P. Doctor, F.G. De Mello, Stable complexes involving acetylcholinesterase and amyloid-ß peptide change the biochemical properties of the enzyme and increase the neurotoxicity of Alzheimer's fibrils, J. Neurosci. 18 (1998) 3213–3223.
[7] F.J. Muñoz, N.C. Inestrosa, Neurotoxicity of acetylcholinesterase amyloid ß-peptide aggregates is dependent on the type of Aß peptide and the AChE concentration present in the complexes, FEBS Lett. 450 (1999) 205–209.
[8] M. Mesulam, C. Geula, Butyrylcholinesterase reactivity differentiates the amyloid plaques of aging from those of dementia, Ann. Neurol. 36 (1994) 722–727.
[9] J.R. Atack, E.K. Perry, J.R. Bonham, R.H. Perry, B.E. Tomlinson, G. Blessed, A. Fairbairn, Molecular forms of acetylcholinesterase in senile dementia of Alzheimer type: Selective loss of the intermediate (10S) form, Neurosci. Lett. 40 (1983) 199–204.
[10] T. Arendt, M.K. Brückner, M. Lange, V. Bigl, Changes in acetylcholinesterase and butyrylcholinesterase in Alzheimer's disease resemble embryonic development—a study of molecular forms, Neurochem. Int. 21 (1992) 381–396.
[11] J. Sáez-Valero, G. Sberna, C.A. McLean, D.H. Small, Molecular isoform distribution and glycosylation of acetylcholinesterase are altered in brain and cerebrospinal fluid of patients with Alzheimer's disease, J. Neurochem. 72 (1999) 1600–1608.
[12] M.-S. García-Ayllón, D.H. Small, J. Avila, J. Sáez-Valero, Revisiting the role of acetylcholinesterase in Alzheimer's disease: cross-talk with P-tau and ß-amyloid, Front. Mol. Neurosci. 4 (2011) 22.
[13] M.-S. García-Ayllón, I. Riba-Llena, C. Serra-Basante, J. Alom, R. Boopathy, J. Sáez-Valero, Altered levels of acetylcholinesterase in Alzheimer plasma, PLoS One 5 (2010), e8701.
[14] H. Dvir, I. Silman, M. Harel, T.L. Rosenberry, J.L. Sussman, Acetylcholinesterase: from 3D structure to function, Chem. Biol. Interact. 187 (2010) 10–22.

[15] J. Wiesner, Z. Kríž, K. Kuca, D. Jun, J. Koca, Acetylcholinesterases–the structural similarities and differences, J Enzyme Inhib. Med. Chem. 22 (2007) 417–424.
[16] A. Chatonnet, O. Lockridge, Comparison of butyrylcholinesterase and acetylcholinesterase, Biochem. J. 260 (1989) 625–634.
[17] Y. Dudai, I. Silman, The molecular weight and subunit structure of acetylcholinesterase preparations from the electric organ of the electric eel, Biochem. Biophys. Res. Commun. 59 (1974) 117–124.
[18] T.L. Rosenberry, D. Scoggin, Structure of human erythrocyte acetylcholinesterase. Characterization of intersubunit disulfide bonding and detergent interaction, J. Biol. Chem. 259 (1984) 5643–5652.
[19] Y. Nicolet, O. Lockridge, P. Masson, J.C. Fontecilla-Camps, F. Nachon, Crystal structure of human butyrylcholinesterase and of its complexes with substrate and products, J. Biol. Chem. 278 (2003) 41141–41147.
[20] J. Cheung, M.J. Rudolph, F. Burshteyn, M.S. Cassidy, E.N. Gary, J. Love, M. C. Franklin, J.J. Height, Structures of human acetylcholinesterase in complex with pharmacologically important ligands, J. Med. Chem. 55 (2012) 10282–10286.
[21] Schrödinger Release 2018, LigPrep, Schrödinger, LLC, New York, NY, 2018.
[22] The PyMOL Molecular Graphics System Version 2.0 Schrödinger, LLC.
[23] Schrödinger Release 2018, Desmond Molecular Dynamics System, D. E. Shaw Research, New York, NY, 2018. Maestro-Desmond Interoperability Tools, Schrödinger, New York, NY, 2018.
[24] M. Turner, J. McKinnon, S. Wolff, D. Grimwood, P. Spackman, D. Jayatilaka, M. Spackman, CrystalExplorer17, The University of Western Australia Australia, 2017.
[25] M.J. Frisch, G.W. Trucks, H.B. Schlegel, G.E. Scuseria, et al., Gaussian 09 Package, Gaussian Inc, Pittsburgh PA, 2009.
[26] P. Macchi, L.J. Farrugia, C. Gatti, P. Mallinson, T. Richter, T. Koritsanszky, A. Volkov, XD2016, 2016.
[27] T. Lu, F. Chen, Multiwfn: a multifunctional wavefunction analyzer, J. Comput. Chem. 33 (2012) 580–592.
[28] G. Saleh, L. Lo Presti, C. Gatti, D. Ceresoli, NCImilano: an electron-density-based code for the study of noncovalent interactions, J. Appl. Crystallogr. 46 (2013) 1513–1517.
[29] C.B. Hübschle, P. Luger, MolIso–a program for colour-mapped iso-surfaces, J. Appl. Crystallogr. 39 (2006) 901–904.
[30] V.K. Gupta, R. Pal, N.J. Siddiqi, B. Sharma, Acetylcholinesterase from human erythrocytes as a surrogate biomarker of lead induced neurotoxicity, Enzyme Res. 2015 (2015).
[31] G.L. Ellman, K.D. Courtney, V. Andres Jr., R.M. Featherstone, A new and rapid colorimetric determination of acetylcholinesterase activity, Biochem. Pharmacol. 7 (1961) 88–95.
[32] H. Lineweaver, D. Burk, The determination of enzyme dissociation constants, J. Am. Chem. Soc. 56 (1934) 658–666.
[33] M. Dixon, The determination of enzyme inhibitor constants, Biochem. J. 55 (1953) 170–171.
[34] L. Chitra, C.R. Kumar, H.M. Basha, S. Ponne, R. Boopathy, Interaction of metal chelators with different molecular forms of acetylcholinesterase and its significance in Alzheimer's disease treatment, Proteins: Struct, Funct. Bioinf. 81 (2013) 1179–1191.
[35] D. Barak, A. Ordentlich, A. Bromberg, C. Kronman, D. Marcus, A. Lazar, N. Ariel, B. Velan, A. Shafferman, Allosteric modulation of acetylcholinesterase activity by peripheral ligands involves a conformational transition of the anionic subsite, Biochemistry 34 (1995) 15444–15452.
[36] A.E. Reyes, D.R. Perez, A. Alvarez, J. Garrido, M.K. Gentry, B.P. Doctor, N. C. Inestrosa, A monoclonal antibody against acetylcholinesterase inhibits the formation of amyloid fibrils induced by the enzyme, Biochem. Biophys. Res. Commun. 232 (1997) 652–655.
[37] M. Bartolini, C. Bertucci, V. Cavrini, V. Andrisano, ß-Amyloid aggregation induced by human acetylcholinesterase: inhibition studies, Biochem. Pharmacol. 65 (2003) 407–416.
[38] P.P. Venugopal, M. Shilpa, D. Chakraborty, Theoretical insights into molecular mechanism and energy criteria of PARP-2 enzyme inhibition by benzimidazole analogues, Proteins: Struct., Funct., Bioinf. (2021). In press.
[39] K. Saravanan, M. Sivanandam, G. Hunday, L. Mathiyalagan, P. Kumaradhas, Investigation of intermolecular interactions and stability of verubecestat in the active site of BACE1: development of first model from QM/MM-based charge density and MD analysis, J. Biomol. Struct. Dyn. 37 (2019) 2339–2354.
[40] R.N. Devi, A.D. Stephen, P. Justin, K. Saravanan, P. Macchi, C. Jelsch, Topological and electrostatic properties of diclofenac molecule as a non-steroidal anti-inflammatory drug: an experimental and theoretical study, J. Mol. Struct. 1196 (2019) 42–53.
[41] K. Saravanan, P. Kumaradhas, Acylguanidine-BACE1 complex: insights of intermolecular interactions and dynamics, J. Theor. Biol. 464 (2019) 33–49.
[42] K. Saravanan, G. Hunday, P. Kumaradhas, Binding and stability of indirubin-3-monoxime in the GSK3ß enzyme: a molecular dynamics simulation and binding free energy study, J. Biomol. Struct. Dyn. 38 (2020) 957–974.
[43] S.K. Mandal, P. Saha, P. Munshi, N. Sukumar, Exploring potent ligand for proteins: Insights from knowledge-based scoring functions and molecular interaction energies, Struct. Chem. 28 (2017) 1537–1552.
[44] L. Huang, L. Massa, J. Karle, Kernel energy method illustrated with peptides, Int. J. Quantum Chem. 103 (2005) 808–817.
[45] S.K. Mandal, B. Guillot, P. Munshi, Electron density based analysis of NH··· O= C hydrogen bonds and electrostatic interaction energies in high-resolution secondary protein structures: insights from quantum crystallographic approaches, CrystEngComm 22 (2020) 4363.